THE SOLAR-SURFACE BOUNDARY CONDITIONS OF CORONAL MAGNETIC LOOPS

Y. MOK and G. VAN HOVEN
Department of Physics, University of California, Irvine, CA 92717, U.S.A.

(Received 10 March, 1994; in revised form 29 May, 1995)

Abstract. The dynamical properties of a realistic *thermal-structure* interface between a coronal loop and the chromosphere/photosphere are investigated by numerical simulations using acoustic and Alfvénic excitations. These properties are relevant to the end conditions seen by coronal MHD perturbations (e.g., waves or instabilities), in the absence of much slower energetics effects. Analytic studies of coronal-loop hydromagnetics have often made simplifying assumptions about the boundary conditions at the loop base in order to make their calculations tractable. However, in the presence of a transition region and chromosphere with rapidly varying plasma conditions, it is not clear how valid these heuristic assumptions are. In this study, we find that the discontinuous fluid-density model approximately represents the reflection/ transmission scaling with respect to varying transition-region density and temperature (i.e., dynamic impedance) ratios, although it does not quantitatively predict the chromospheric response to wave-like coronal activity. This disagreement is partially due to the finite width of the corona-to-photosphere transition.

1. Introduction

Coronal loops (Priest, 1978; Van Hoven, 1981) have been well observed since the *Skylab* mission in the 1970's. They are loop-like, semi-toroidal magnetic structures in the corona with footpoints anchored in the photosphere. After numerous studies, they are now widely believed to be plasma loops with temperatures and densities different from their surroundings and, therefore, having distinctive radiation signatures. A combination of observations and analyses also show that these loops are aligned with the local magnetic field. Although their origin and formation processes are still not fully understood, their basic properties and internal structures have been investigated in some detail.

In the treatment of the magnetohydrodynamic (MHD) properties of these loops, especially of their stability, one of the difficulties is how to treat the interaction between the hot and diffuse coronal-loop plasma and the cool and dense surface layers at the footpoints, both of which are threaded by the same magnetic field lines. Most previous studies have described the ends of the loops as being imbedded in the 'photosphere', selected as the approximate position (in a view from high in the corona) where the density takes a quasi-step-function jump and thus all velocities decrease. (However, see the note, citing a T. E. Holzer comment, on p. 822 of Migliuolo and Cargill (1983).) In this paper we will look at the dynamic effects of a moderately realistic energetically consistent model of this *distributed* boundary *layer* in more detail. Previous idealized treatments of the coronal boundary have

Solar Physics **161:** 67–81, 1995.

included simple forms of the transition region (TR) and chromosphere/photosphere (Leer, Holzer, and Fla, 1982; Hollweg, 1984a, b).

The underlying *density/temperature* structure of a coronal loop arises as the result of a complicated energy balance between heating, thermal conduction and radiative cooling (Oran, Mariska, and Boris, 1982). In the coronal part, heating is balanced by the divergence of the thermal flux as radiative cooling has only a minor effect (Mok, Schnack, and Van Hoven, 1991), primarily because of the large thermal conductivity. While all three energy-transport effects have comparable influence on the thermal structure in the middle of the transition region, the balance is primarily between heat-flux divergence and radiative cooling in the chromosphere. The fact that coronal loops have a lifetime longer than other relevant time scales, except resistive diffusion, suggests that they are indeed in thermal and force equilibrium.

However, since the loop is in contact with the solar surface, which acts like a large mass and energy reservoir determining density and temperature at the footpoints, the loop is not truly isolated. Assuming that the magnetic field lines extend below the transition region (TR) smoothly without kinks, the 'loop' can be considered to penetrate into the chromosphere and photosphere as well (Zweibel, 1985). This poses a problem concerning the MHD identity of the loop. Where does it begin and how sensitively do the resulting dynamical loop properties depend on the boundary location one uses in an analysis? A commonly used compromise is to model the dynamic properties of the photosphere-corona transition by a set of 'boundary conditions' presented to the coronal part of the loop. This approach, though widely used, has led to controversy concerning what kind of magnetodynamic boundary conditions are most appropriate (An, 1984).

The simplest of these models considers only the coronal part as the loop, with the boundary put at the coronal base, where the density 'jump' occurs. It assumes that the chromosphere and photosphere below this point are so dense and sluggish that any dynamic activity originating from the corona must stop at the boundary. This crude requirement (Hood and Priest, 1979), sometimes called the *rigid-wall* condition, demands that *all* perturbed dynamical quantities, such as velocity and magnetic field, vanish at the loop base. This may be a convenient way to simplify the analysis, but it is a strong constraint condition which overestimates MHD stability (An, 1984).

A slightly less restrictive model, called the *line-tied* condition (effectively *equivalent to* that at a perfect conductor; Van Hoven, Ma, and Einaudi, 1981; Migliuolo, Cargill, and Hood, 1984; Mikić, Schnack, and Van Hoven, 1990), allows the plasma to flow along the equilibrium magnetic field across the boundary (while conserving energy globally), but forbids flow perpendicular to the magnetic field. This arises from the realization that it requires less energy for the plasma to flow along the field than across it because the fluid motion does not have to perturb the strong equilibrium field. In particular, Einaudi and Van Hoven (1981) argued, in the context of a variational calculation, that our lack of physical knowledge below the surface dic-

tates the use of the least restrictive boundary constraint, a 'flow-through' condition which conserves energy.

There is yet another simple model, which we will call the *discontinuous* model, which assumes that the density and temperature profiles of the loop have a discontinuity at the location of the TR, which is replaced by a jump in density/temperature (Hollweg, 1984b), which one could consider to be the loop base. In this case, one can derive dynamic boundary conditions in terms of impedances or group velocities (Jackson, 1975). A drawback of this model is that it requires the knowledge or specification of perturbation behavior below the (opaque) solar surface (Zweibel, 1985).

In this work, we attack this dynamic 'boundary' problem in a higher level of approximation by numerically solving the energetically modified magnetohydrodynamic equations over a domain from the coronal apex to deep in the chromosphere. This approach allows us to incorporate many factors that are realistic yet too complicated to be treated by analytic models. The validity of these commonly used analytic models will also be tested. Our emphasis will be on excitations of the *long-period* (long-wavelength) variety which can arise in the corona from slow external wave excitations or internally near the crucial marginal point ($\partial/\partial t \rightarrow 0$) in a (compressible) MHD stability analysis (Van Hoven, 1981). (In either case, their periods cannot be so long that their wavelengths do not fit within the coronal loop length.)

2. Model Equations and Equilibria

To study the dynamic response of a realistic corona-chromosphere interface to activity within a magnetic loop, a stable density/temperature structure for the atmosphere must first be established. Using the method described in our previous work (Mok *et al.*, 1990), we have obtained a series of loop equilibria with different coronal densities and pressures. Although some of these configurations may not correspond to realistic solar conditions, the purpose of investigating a range of equilibria is to study the dependence of the subsequent dynamic responses on the relevant physical properties, such as acoustic and Alfvén (group) speeds. Their scaling will hopefully reveal how the actual solar surface differs from a rigid wall or a discontinuous fluid boundary. We obtained the energy and force equilibria by advancing the following set of equations until they relax to a steady state.

The equation governing the temperature is given by

$$2nk\left(\frac{\partial T}{\partial t}+v\frac{\partial T}{\partial x}\right)=-2nk(\gamma-1)T\frac{\partial v}{\partial x}+$$

$$+(\gamma-1)\left[H-n^2\phi(T)+\frac{\partial}{\partial x}\kappa\frac{\partial T}{\partial x}\right], \qquad (1)$$

where T, n, p, v are temperature, electron number density, pressure ($= 2nkT$), and (parallel) fluid velocity, respectively. $\phi(T)$ is the radiative energy loss (Athay, 1986) with a rapid, but smooth, low-temperature cut-off at 2×10^4 K to simulate the effects of optical thickness. Although we chose one of the many available forms of ϕ, its specific functional form is not critical in this application. H is the heating function, taken to be uniform, and κ is the classical parallel (to $\mathbf{B}$) thermal conductivity ($\sim T^{5/2}$) given by Braginskii (1965).

As a numerical technique, described in Mok, Schnack, and Van Hoven (1990), an artificial density source of limited extent is added to the end section of the loop in the continuity equation in order to impose the desired density and scale height at chromospheric temperatures. (This tactic produces a region similar to that used by Hollweg (1984a) to model the boundary conditions of a constant-scale-height 'photosphere' (without a transition-region jump).) We take care to ensure that there is a real chromosphere in the final solution; i.e., there is a finite-length region beyond the artificial source with a uniform temperature at $T_c \sim 2 \times 10^4$ K. In all of the equilibria described in the next section, the artificial density source occupies the region from 0 to $0.1L$, where L is the total length of the simulation. Typically, the transition region is located at 0.2 L - 0.3 L, below which the temperature is uniform at a nominal chromospheric value. The region beyond 0.1 L and below the transition region can be considered as a natural chromosphere because it satisfies the physical continuity equation (source $= 0$) and has all the desired chromospheric properties. The continuity equation, therefore, has the form

$$\frac{\partial \rho}{\partial t} + \frac{\partial}{\partial x}(\rho v) = -\nu[\rho - \rho_c] \,, \tag{2}$$

where ρ_c is the chromospheric density (including scale-height effects at T_c when gravity is included), and ν is finite only within the artificial density source and zero otherwise. The momentum equation is given by

$$\rho\left(\frac{\partial v}{\partial t} + v\frac{\partial v}{\partial x}\right) = -\frac{\partial p}{\partial x} + \rho g_{\|} - \frac{1}{4\pi} B_{\perp} \frac{\partial B_{\perp}}{\partial x} \,, \tag{3}$$

where $g_{\|}$ is gravity projected along the loop. The last term reflects the influence of the emulated perpendicular magnetic field in the 1.5-D model (Van Hoven, Mok, and Drake, 1992), and will be discussed in Section 3.2. Two sets of equilibria are obtained, one with full solar gravity projected along the semi-circular loop and the other without gravity. We distinguish these two cases because they have different thermal structures, resulting in different variations in acoustic and Alfvén speeds along the loop. The system of Equations (1)–(3) is advanced in time until it relaxes to a steady state. Only half of the loop is used in the computation, and symmetry is assumed. The temperature-density profile of a typical case is shown in Figure 1.

The first set of equilibria, with gravity, consists of three cases:

(a) $T_a = 1.04 \times 10^6$ K, $\rho_a = 1.48 \times 10^{-15}$ g cm^{-3}, $\rho_b = 9.34 \times 10^{-14}$ g cm^{-3};

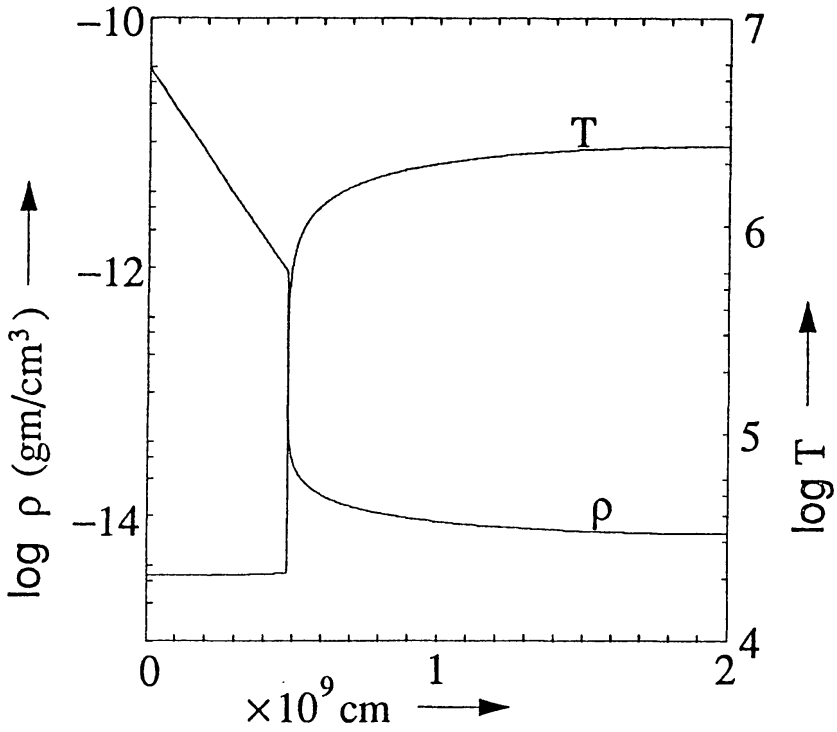

Fig. 1. Typical equilibrium density and temperature profiles (Case (b) of (4)), with scales at left and right, respectively. The temperature in the chromosphere is 2×10^4 K, as specified by the radiative cooling cut-off, and the source parameter (ν in Equation (2)) is zero above $x = 0.2$. The density in the isothermal chromosphere falls exponentially due to full solar gravity.

(b) $T_a = 2.40 \times 10^6$ K, $\rho_a = 7.11 \times 10^{-15}$ g cm^{-3}, $\rho_b = 1.00 \times 10^{-12}$ g cm^{-3} (cf., Figure 1);

(c) $T_a = 9.41 \times 10^6$ K, $\rho_a = 1.06 \times 10^{-13}$ g cm^{-3}, $\rho_b = 5.00 \times 10^{-11}$ g cm^{-3}, where T_a, ρ_a, and ρ_b are apex temperature, apex density and base density, respectively.

Base temperature is fixed approximately at the radiation cut-off (2×10^4 K) in all cases. Note that the stated base density is the value at the location where the temperature reaches the chromospheric value from above rather than the value at the end point ($x = 0$) of the computation. For chromospheric responses to longitudinal fluid motions in the corona, the relevant parameter is the ratio of apex to base acoustic speeds. In these three cases, they are

$$\frac{c_a}{c_b} = \left(\frac{T_a}{T_b}\right)^{1/2} = 7.02,\ 10.76,\ 21.42,\ \text{respectively}\,, \tag{4}$$

chosen to bracket the nominal solar value.

The second set of equilibria consists of two loops without gravity: (a) $T_a = 1.29 \times 10^6$ K, $\rho_a = 1.38 \times 10^{-15}$ g cm^{-3}, $\rho_b = 2.37 \times 10^{-14}$ g cm^{-3}; and (b) $T_a = 2.27 \times 10^6$ K, $\rho_a = 7.66 \times 10^{-16}$ g cm^{-3}, $\rho_b = 8.36 \times 10^{-14}$ g cm^{-3}. Their apex-to-base ratios of acoustic speeds are

$$\frac{c_a}{c_b} = \left(\frac{T_a}{T_b}\right)^{1/2} = 7.75,\ 10.40,\ \text{respectively}\,. \tag{5}$$

These density/temperature equilibria will be used as initial conditions in the dynamic cases of Sections 2.1 and 3.2.

3. Perturbations and Responses

In the conventional treatment of coronal loops, especially analytic stability studies, one often simplifies the model by lumping all of the transition-region and chromospheric effects into the 'photospheric boundary' confining the hot, tenuous coronal plasma (Hood and Priest, 1979; Van Hoven, Ma, and Einaudi, 1981; An, 1984; Hood, 1986; Mikić, Schnack, and Van Hoven, 1990). However, using such a heuristic boundary condition to simulate this interface may not be as realistic as one would like. This is primarily due to the facts that (a) the chromosphere is not infinitely massive, and (b) the coronal plasma does not directly interface with the cool, dense photosphere, but connects through a finite-width transition region (TR) and a 2000 km deep chromosphere where the *energetics* (and ρ and T) change continuously, but dramatically, from one side to the other (Oran, Mariska, and Boris, 1982; Mok, Schnack, and Van Hoven, 1991). This buffer region therefore presents a diffuse boundary to coronal excitations. In fact, McClymont and Craig (1985), and Antiochos et al. (1985) argued (for energy-transport excitations) that the loop base should be put deep in the chromosphere because the plasma there is effectively uniform, so that the boundary's exact location is immaterial. Arguments of this kind imply that any analysis of the loop must include the highly inhomogeneous transition region (Zweibel, 1985) whose sharp density/temperature gradients are usually avoided by researchers in order to keep the calculation tractable. Hollweg has considered two aspects of this boundary-condition problem with separate treatments of a chromosphere/photosphere-like exponential-density ramp (Hollweg, 1984a) and of a TR-like density step (Hollweg, 1984b).

The problem we are prepared to investigate is how a realistic corona-photosphere interface is similar or dissimilar to these frequently used, heuristic, boundary conditions, taking into account factors which are inherent in the solar atmosphere, especially the transition region, such as radiative energy loss and gravity. In this section, we will study two types of fluid perturbations that are often excited by a variety of coronal activities. Once again, our emphasis is on *long-wavelength* perturbations of the variety encountered in *full-loop* magnetic kinks or pressure oscillations.

The first type is *longitudinal* motions propagating primarily at the *acoustic* speed. Assuming that the plasma is confined by a strong magnetic field, this fluid motion can be considered as one-dimensional, i.e., along the loop magnetic-field geometry. Although the chromosphere has a much higher mass density and lower temperature, the corona–chromosphere interface cannot be considered as totally

rigid because the acoustic speed is proportional to the square root of the temperature. Typically, the ratio of sound speeds is ~ 10, sufficient to have significant transmission through the interface. The low-frequency modes can further be affected, although perhaps in a less important way, by the effect of the radiative energy loss ($\sim n^2\phi$), whose time scale significantly decreases in the lower TR and becomes comparable to those of the acoustic waves (Oran, Mariska, and Boris, 1982).

The second type of perturbation is Alfvénic transverse waves. Analogous to the acoustic waves, the Alfvén speed is inversely proportional to the square root of density, and changes by a factor of ~ 10 across the transition region. As a result, we can reasonably expect that the chromosphere will not behave like a rigid wall to the plasma motions of the wave, and the transmission may not be totally negligible.

3.1. Longitudinal (acoustic) perturbations

Starting from an equilibrium, we add a linear velocity perturbation to the coronal part of the loop. The perturbation is of sinusoidal shape and has a wavelength slightly shorter than the coronal part of the loop length. In order to diagnose the plasma motions and other properties, we put two probes at different locations in the loop. One is located in the corona just outside the initial velocity perturbation. The wave packet propagates past this probe before reaching the chromosphere. The second probe is located just inside the chromosphere, which is taken to begin at the position where the temperature becomes uniform. In the following, we will compare the plasma motions at these two locations in order to understand how the plasma just below the 'boundary', i.e., at the second probe, responds to the incident coronal plasma motions as measured by the first probe.

Under the 'rigid wall' boundary-condition model, the plasma motion at the second probe should vanish by definition. The line-tied and the discontinuous interface conditions are actually the same in this case since the system is one-dimensional, implying a strong, uniform, constant, magnetic field in the direction of the plasma motion. A simple exercise of matching the wave solutions without gravity at the boundary (assumed discontinuous) shows that the predicted 'transmission' ratio of velocity amplitudes is given by

$$\tau_d \equiv \frac{v(\text{chromosphere})}{v(\text{corona})} = \frac{2\alpha}{1+\alpha}\,, \tag{6}$$

where α ($= c_s(\text{chromosphere})/c_s(\text{corona})$) is the ratio of acoustic (group) speeds (Jackson, 1975). (We have chosen τ_d as a straightforward (and easy to determine) characterization of the effective boundary 'jump' conditions; one could equally have chosen the related 'reflection' coefficient.)

Figure 2 shows the time profiles of the longitudinal velocities at the two probes in the simulation for the equilibrium atmosphere shown in Figure 1. The time delay between the arrival at the two probes is approximately equal to the distance between the probes divided by the average acoustic speed. As the wave packet

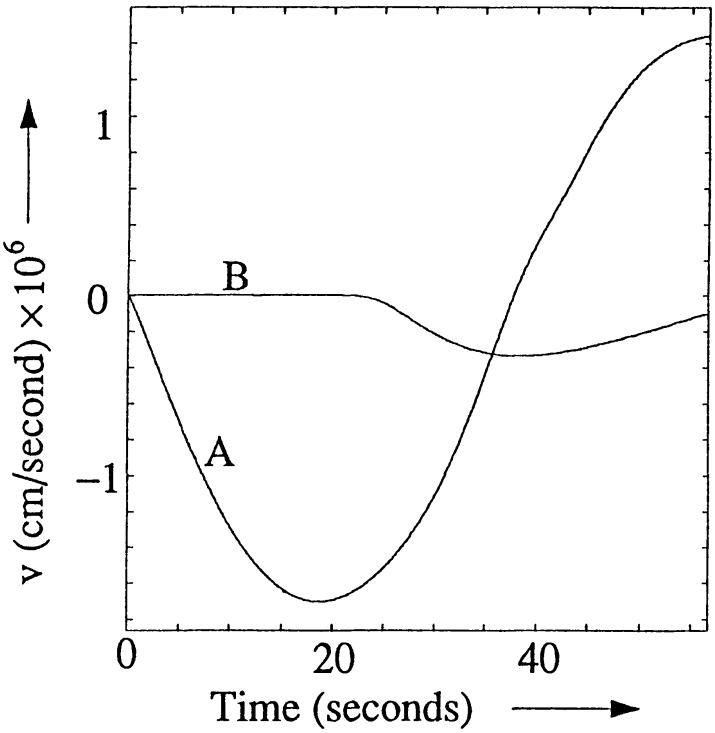

Fig. 2. Velocities at two locations responding to a longitudinal (downward) acoustic perturbation to the equilibrium shown in Figure 1. Curve A is measured at the location 8×10^8 cm, representing the fluid velocity in the corona. Curve B is measured at 4.6×10^8 cm, just inside the chromosphere where the temperature is quasi-uniform. The time delay between the peaks of the two curves is the time it takes for the wave to travel from the coronal probe to the chromospheric probe.

travels downward from the corona, it is partially reflected by the TR. However, a non-negligible amount is transmitted into the chromosphere, as indicated by the fluid velocity registered at the chromospheric probe. This finite velocity amplitude shows that the realistic corona-chromosphere interface does not behave like a rigid wall. The measured ratio τ_m of the two velocity amplitudes is 0.143, which is also different from the value of $\tau_d = 0$ or 0.170 predicted by the other two models.

This is not entirely unexpected since the predicted value is based on a simple configuration consisting of two different, but homogeneous, media with a sharp boundary and without gravity. In the present case, there is a finite region where temperature decreases from coronal to chromospheric values. The *averaged* temperature ratio, therefore, is lower than that in the simple discontinuous model. Moreover, due to the presence of gravity, plasma density rises rapidly beginning at the chromosphere. The increased inertia in the neighborhood of the TR tends to further reduce the response as compared to the simple model. From these two numbers, we can conclude that the actual, continuous, chromosphere-corona interface is more rigid than these models predict.

The direct effects of the radiative energy loss in the lower TR on the dynamic response are more difficult to isolate for analysis, since it is not possible to form a realistic thermally structured atmosphere without radiative cooling. However, we

TABLE I

Transmission properties of sound waves in a gravitating TR

T(corona)	1.04×10^6 K	2.40×10^6 K	9.41×10^6 K
$\tau_m = v$(chromosphere)/v(corona)	0.223	0.143	0.0775
$\alpha = [T$(chromosphere)/T(corona)$]^{1/2}$	0.143	0.0929	0.0467
$\tau_d = \dfrac{2\alpha}{1+\alpha}$	0.250	0.170	0.0892
τ_m/τ_d	0.892	0.841	0.869

believe that it is of secondary importance because the radiative cooling time in the corona is much longer than the dynamic time scale. The lower transition region, where the cooling time is short enough to be important, spans only a narrow layer whose length is much shorter than the wavelength. Radiative cooling in the present calculation simply provides an energy sink for the heat flow from the corona to maintain the thermal structure at equilibrium.

In order to investigate the general, acoustic-excitation, transmission properties of this interface, we compute the responses for several equilibria, as described in Section 2, which differ in coronal temperature but are otherwise identical. The chromospheric temperature remains at 2×10^4 K in all cases. Although some of these cases may not correspond to a real condition of the solar atmosphere, the purpose is to study how the dynamic responses scale with the acoustic speed as compared to other models. In each of these cases, perturbations of the same wavelength and amplitude are excited in the upper coronal part of the loop. Table I shows the computed results, the square root of T(chromosphere)/T(corona), as well as other relevant parameters. All cases have full solar gravity. Although the three cases have drastically different physical conditions with different responses to the perturbations from the corona, the ratio τ_m/τ_d of the actual velocity ratio to the predicted density-step-function ratio τ_d (from (6)) remains approximately constant to within 6%.

For comparison purposes, we also have computed the dynamic responses for equilibria without gravity, as shown in Table II. In these cases, the force balance of the loop is distinctively different, resulting in different thermal structures which have uniform pressures and generally greater lengths. Without the density rise in the chromosphere, the responses at the boundary are less rigid compared to the simple step-discontinuity model because of the lower average temperature. The ratio τ_m/τ_d, however, is constant to within 1%.

From these results, one can see that, although the actual chromospheric responses are not predicted by any one of the theoretical models, their scaling generally agrees with the transmission ratios determined by the dynamic-impedance or group-velocity values of the discontinuous-fluid/line-tied models.

TABLE II

Transmission properties of sound waves through a TR with $g = 0$

T(corona)	1.29×10^6 K	2.27×10^6 K
$\tau_m = v$(chromosphere)/v(corona)	0.256	0.197
$\alpha = [T$(chromosphere)/T(corona)$]^{1/2}$	0.129	0.0962
$\tau_d = \frac{2\alpha}{1+\alpha}$	0.229	0.175
τ_m/τ_d	1.118	1.126

3.2. TRANSVERSE (MAGNETIC) PERTURBATIONS

Using the method described in our previous work (Van Hoven, Mok, and Drake, 1992), we can extend the 1-D model equations into a 1.5-D calculation by adding two equations governing the evolution of the 'perpendicular' velocity and magnetic field in order to emulate the transverse dynamics:

$$\rho \frac{\partial v_\perp}{\partial t} = \frac{B_0}{4\pi}\frac{\partial B_\perp}{\partial x} - \rho v \frac{\partial v_\perp}{\partial x} + \rho g_\perp \,, \tag{7}$$

$$\frac{\partial B_\perp}{\partial t} = B_0 \frac{\partial v_\perp}{\partial x} - \frac{\partial}{\partial x}(B_\perp v) \,, \tag{8}$$

which is derived from the perpendicular components of the MHD equations. Gravity is projected into a semi-circular equilibrium-field loop as described in Section 2. The magnetic fields in the cases treated are chosen in such a way that the plasma β in the corona remains the same at 2.0×10^{-2} in all cases. A linear perturbation in $B_\perp$ is launched from the upper half of the loop in the same way that the acoustic wave was excited in the last section, with the same wavelength and the same launch site. The Alfvénic perturbation propagates downward, passing the first probe to reach the base. The two probes are at the same locations as before. The *perpendicular* fluid *displacements* ξ at the two probes are measured by the time integrals of the perpendicular velocities $v_\perp$ at the respective sites.

Figure 3 shows the time profiles of the perpendicular fluid displacements in a loop with $B = 60$ G, $T_a = 2.4 \times 10^6$ K (equivalent to case (b) of (4)), and a half-length (from apex to chromosphere) of 1.54×10^4 km. The wave packet first passes the upper probe, as indicated by the higher curve. It then reaches the chromosphere and is partially transmitted as indicated by the lower response curve registered by the second probe. The ratio of the two amplitudes is 0.195. It is quite clear that the chromosphere, even with its large mass density, does not behave like a rigid wall. The line-tied model in this case actually leads to the same condition as the rigid wall because it does not allow plasma to flow across the equilibrium magnetic field, implying that the *perpendicular* fluid displacement at the TR boundary should vanish. The discontinuous fluid model (Hollweg, 1984b) predicts the ratio to be

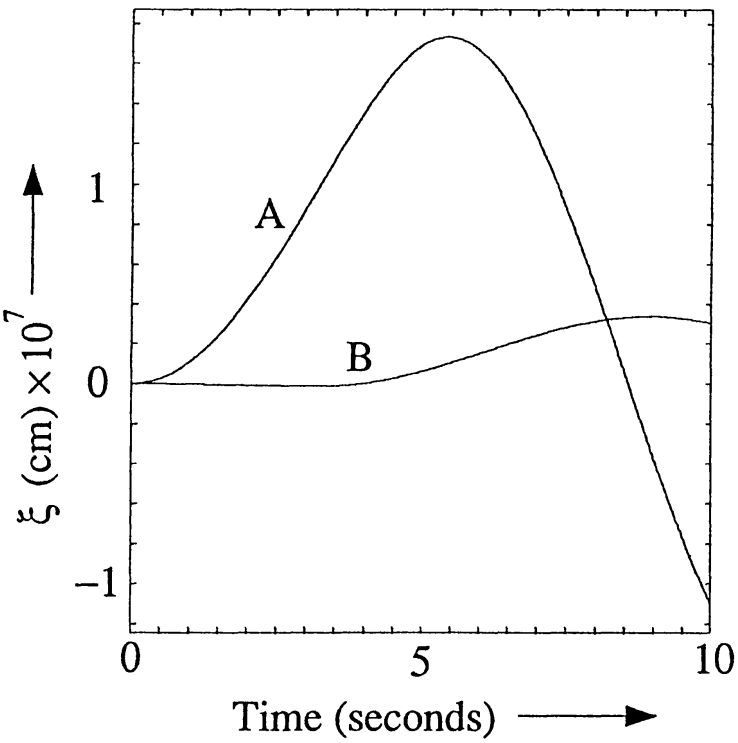

Fig. 3. Perpendicular fluid displacements measured at two locations responding to an Alfvénic perturbation to the equilibrium shown in Figure 1. The probes are located in the same positions as in Figure 2. Curve A is for the corona and Curve B is for the upper chromosphere.

$$\tau_d = \frac{2\alpha_A}{1+\alpha_A}, \tag{9}$$

where

$$\alpha_A = \left[\frac{\rho(\text{corona})}{\rho(\text{chromosphere})}\right]^{1/2} \tag{10}$$

is the ratio of Alfvén speeds. For this case $\tau_d = 0.156$.

In order to study the scaling of the response according to the Alfvén-speed ratio, we have computed the perpendicular response ratios for the several equilibria of Section 2 with different coronal densities, all of which have solar gravity projected onto a semi-circular loop. The results are shown in Table III. Two test cases were also computed without gravity, with the results shown in Table IV.

From these two tables, one can see that the responses scale according to the τ_d value in the same manner as the discontinuous fluid model, although the results are not quantitatively predicted. The ratio τ_m/τ_d is constant to within 3%. The reason for the difference is the same as the one for the longitudinal case; namely, the Alfvén speed varies rapidly, but continuously, with density through the lower corona and the transition region. The average Alfvén speed in this region is lower than that of the simple discontinuous model, leading to a less rigid boundary. The rigid wall and the line-tied model, however, do not seem to be appropriate.

TABLE III

Transmission properties of Alfvén waves in a gravitating TR

ρ(corona)	1.48×10^{-15} g cm^{-3}	7.11×10^{-15} g cm^{-3}	1.06×10^{-13} g cm^{-3}
$\tau_m = \xi$(chromosphere)/ξ(corona)	0.287	0.195	0.113
$\alpha_A = [\rho(\text{corona})/\rho(\text{chromosphere})]^{1/2}$	0.126	0.0843	0.0461
$\tau_d = \dfrac{2\alpha_A}{1+\alpha_A}$	0.224	0.1555	0.0881
τ_m/τ_d	1.281	1.254	1.283

TABLE IV

Transmission properties of Alfvén waves through a TR with $g = 0$

ρ(corona)	1.38×10^{-15} g cm^{-3}	7.66×10^{-16} g cm^{-3}
$\tau_m = \xi$(chromosphere)/ξ(corona)	0.279	0.219
$\alpha_A = [\rho(\text{corona})/\rho(\text{chromosphere})]^{1/2}$	0.1284	0.0957
$\tau_d = \dfrac{2\alpha_A}{1+\alpha_A}$	0.2275	0.1747
τ_m/τ_d	1.226	1.254

4. Summary and Discussion

Because the physical parameters of the hot, tenuous, coronal plasma and the cool, dense photosphere are drastically different, their interactions, through a relatively thin layer formed by the transition region and chromosphere, are quite complicated. In analyzing the dynamics of coronal loops, the photosphere, chromosphere and transition region are often grouped together as a single component (except see Hollweg (1984a)), and assumed to present a simple 'boundary condition' to the corona. However, there has not been a consensus on what kind of MHD boundary condition should be used in order to closely approximate the behavior of this transition to the photosphere. The usual heuristic assumption leads to the most commonly used rigid-wall boundary condition (e.g., Hood and Priest, 1979) which requires all perturbed quantities to vanish. Since this is a very restrictive condition, equivalent to an infinitely massive, perfectly conducting chromosphere, the next step closer to reality is to give the plasma some degree of freedom to respond to the dynamic activity propagating downward from the corona. The line-tied condition (e.g., Van Hoven, Ma, and Einaudi, 1981), which allows the plasma to move only

along the magnetic field, and the discontinuous-density model (Hollweg, 1984b) are plausible candidates for a better approximation.

Unfortunately, the actual density and temperature structure is the result of a complicated, slowly adjusting, energy balance between heating, thermal conduction and radiative cooling, and does not have a simple, intuitive functional form ready for an analytic study. A WKB approximation cannot be used because of the short length scale of the transition region. Consequently, a numerical simulation seems to be necessary. In this study, we have investigated the compressible hydromagnetic response of the corona-to-chromosphere transition region under realistic solar conditions, namely, a self-consistent, complete atmosphere, which extends from the isothermal chromosphere to the corona with local energy balance at all heights. In this way the dynamic properties of the highly inhomogeneous transition region are preserved. Assuming a strong magnetie field along the loop, we divide the plasma motions into two classes: longitudinal and transverse. The former are carried mostly by acoustic waves while the latter are Alfvénic. The plasma is perturbed at the top of the coronal loop. The response at the boundary is measured by the fluid velocity or displacement just inside the isothermal chromosphere. Its amplitude is then compared to the corresponding quantity in the corona. In all cases, the chromospheric responses are significantly different from zero, indicating that the rigid-wall boundary condition is a poor approximation. This is not entirely unexpected since the ratio of the characteristic speeds between the chromosphere and the corona is not small enough to prevent partial transmission, as shown by Equations (6) and (9).

For longitudinal fluid motions, a significant fraction of the acoustic wave energy is transmitted into the chromosphere. The amplitude of the transmitted wave is not exactly what is predicted by the simple discontinuous fluid model. This is partly because the acoustic speed decreases continuously, though rapidly, from the corona. The averaged acoustic speed in the neighborhood of the boundary is substantially below its coronal value, which is used in the discontinuous density model to determine the chromospheric response. This is also partly because of the effect of gravity, which makes the density rise rapidly in the chromosphere in the neighborhood of the boundary. The rising density, in turn, makes the boundary more rigid. In other words, the behavior of the actual boundary is somewhere between a discontinuous fluid and a smoothly varying fluid, which could be shown to have much higher transmission in the WKB limit.

To further investigate the properties of the boundary, we study a series of cases with different corona-to-chromosphere temperature ratios. Although the actual amplitude ratios of the transmitted waves are different from the discontinuous fluid model, their scaling with τ_d (6) agrees to within a few percent as shown in Tables I and II. The line-tied model in this case does not explicitly specify the behavior of the boundary. Therefore, it is not inconsistent with the result.

For transverse fluid motions, which are essentially Alfvénic in the coronal loop, the behavior of the chromospheric plasma is similar to the case of longitudinal

perturbations. Although the Alfvén speed is proportional to the inverse square root of density, as compared to the square root of the temperature for the acoustic speed, the two speeds have similar spatial profiles in most parts of the atmosphere because of the slowly varying pressure controlled by the large gravitational scale height. However, there are basic differences. For instance, the linear Alfvén waves do not compress the plasma. For a negligible density perturbation, the radiative cooling has practically no effect, even below the lower TR where it has a dominant role in the energetics. In all cases, we chose the plasma beta in the corona to be 0.02. In each case, the fluid displacement in the chromosphere exceeds the one predicted by the discontinuous density model. The reason is similar to that in the acoustic case; namely, the Alfvén speed decreases continuously, but rapidly, toward the chromosphere. The averaged Alfvén speed in the lower corona is below its coronal value, which is used in the discontinuous density model. Notice that the line-tied boundary condition in this 1.5-D model predicts a vanishing response. The scaling of the responses was found to agree to within a few percent with τ_d (9) as shown in Tables III and IV.

In conclusion, we have investigated the dynamic (compressible+MHD) behavior of the chromospheric boundary of the corona by 1-D and 1.5-D simulations of a magnetized transition region that is in energy-balance equilibrium. Our results demonstrate that none of the simple, heuristic, boundary conditions can accurately approximate the response of the chromosphere to dynamic coronal excitations under realistic solar conditions. The rigid-wall boundary is too restrictive. The line-tied condition underestimates the plasma motions across the field. The discontinuous density model can give the correct scaling (Jackson, 1975; Hollweg, 1984b), but not the actual amplitude of the response.

Acknowledgements

This research has been supported, in part, by NASA Space Physics Theory, NSF Atmospheric Sciences, and Air Force Phillips Laboratory. Supercomputer access has been provided at NERSC by DOE, and at SDSC by NSF and UCI.

Note Added in Proof

Significant recent progress has been made on the question of the formation of realistic, 3-D, quasi-toroidal, coronal magnetic loops, as described by Van Hoven, Mok, and Mikić (1995, *Astrophys. J.* **440**, L105).

References

An, C.-H.: 1984, *Astrophys. J.* **281**, 419.
Antiochos, S. K, Shoub, E. C., An, C.-H., and Emslie, A. G.: 1985, *Astrophys. J.* **298**, 876.
Athay, R. G.: 1986, *Astrophys. J.* **308**, 975.
Braginskii, S. I.: 1965, *Rev. Plasma Phys.* **1**, 217.
Einaudi, G. and Van Hoven, G.: 1981, *Phys. Fluids* **24**, 1092.
Einaudi, G. and Van Hoven, G.: 1983, *Solar Phys.* **88**, 163.
Hollweg, J. V.: 1984a, *Astrophys. J.* **277**, 392.
Hollweg, J. V.: 1984b, *Solar Phys.* **91**, 269.
Hood, A. W.: 1986, *Solar Phys.* **105**, 307.
Hood, A. W. and Priest, E. R.: 1979, *Solar Phys.* **64**, 303.
Hood, A. W. and Priest, E. R.: 1980, *Astron. Astrophys.* **87**, 126.
Jackson, J. D.: 1975, *Classical Electrodynamics*, Wiley, New York.
Leer, E., Holzer, T. E., and Fla, T.: 1982, *Space Sci. Rev.* **33**, 161.
McClymont, A. N. and Craig, I. J. D.: 1985, *Astrophys. J.* **289**, 820.
Migliuolo, S. and Cargill, P. J.: 1983, *Astrophys. J.* **271**, 820.
Migliuolo, S., Cargill, P. J., and Hood, A. W.: 1984, *Astrophys. J.* **281**, 413.
Mikic, Z., Schnack, D. D., and Van Hoven, G.: 1990, *Astrophys. J.* **361**, 690.
Mok, Y., Schnack, D. D., and Van Hoven, G.: 1991, *Solar Phys.* **132**, 95.
Mok, Y., Drake, J. F., Schnack, D. D., and Van Hoven, G.: 1990, *Astrophys. J.* **359**, 228.
Oran, E. S., Mariska, J. T., and Boris, J. P.: 1982, *Astrophys. J.* **254**, 349.
Priest, E. R.: 1978, *Solar Phys.* **58**, 57.
Priest, E. R. (ed.): 1981, *Solar Flare Magnetohydrodynamics*, Gordon and Breach, London.
Van Hoven, G.: 1981, in Priest (1981), pp. 217-275.
Van Hoven, G., Ma, S. S., and Einaudi, G.: 1981, *Astron. Astrophys.* **97**, 232.
Van Hoven, G., Mok, Y., and Drake, J. F.: 1992, *Solar Phys.* **140**, 269.
Zweibel, E. G.: 1985, *Geophys. Astrophys. Fluid Dyn.* **32**, 317.